Islamic Azad University

**Journal of**

**Optoelectronical Nanostructures**

Spring 2019 / Vol. 4, No. 2

# Numerical Modeling of a Nanostructure Gas Sensor Based on Plasmonic Effect

**Morteza Mansouri[1], Ali Mir[1], Ali Farmani[*,1]**

[1] Faculty of Engineering, Lorestan University, Khoram abad, Iran

(Received 19 Apr. 2019; Revised 18 May 2019; Accepted 26 May 2019; Published 15 Jun. 2019)

**Abstract:** In the present paper, a nanostructure plasmonic gas sensor based on ring resonator structure at the wavelength range of 0.6-0.9 μm is presented. The plasmonic materials/$SiO_2$ with the advantage of high mobility and low loss is utilized as a substrate for structure to obtain some appropriate characteristics for the sensing Performance parameters. To evaluate the proposed sensor and calculation of performance parameters including figure of merit and sensitivity, the effect of the different gas including Carbon Dioxide ($CO_2$), Acetonitrile ($C_2H_3N$), Carbon disulfide, and Sarin are considered. For this purpose 3D-FDTD method is considered. Our calculations show that by coupling between the incident waves and the surface plasmons of the structure, a high transmission ratio of 0.8 and relatively low insertion loss of 6 dB around the wavelength interval of 0.6-0.9 μm are achievable. Furthermore, the calculated sensitivity and figure of merit are 28 and 8.75, respectively. This provides a path for development of nano-scale practical on-chip applications such as plasmonic memory devices.

**Keywords: Plasmonic, Gas sensor, Nanostructure.**

## 1. INTRODUCTION

Environment variation detection play an important role in many optical applications and have been extensively developed during the past few decades [1-20]. A gas sensor is operated through different mechanism including optical, chemical and electrical variations. Generally these sensors operate in two mechanisms: a charge transfer occurs between gas molecules, and the sensitive layer. In other aspect, to enhance of selectivity, efficiency, and reduced noise, nan-scale morphology, surface-to-volume ratio, and quantum confinement should be considered. Footprint, sensitivity, speed, figure of merit, and accuracy are the main common parameters in designing of sensor. To improve the size and speed in each device, nanostructure devices are good candidate. With the continuous development of terahertz (THz) science, much attention has been

* Corresponding author. Email: **Farmani.a@lu.ac.ir**

recently paid to THz technology due to its potential applications in sensing, space sciences, imaging, and wireless communications [21, 22]. In recent years, interest in the development of THz functional devices have attracted, owing to the lack of appropriate response at THz frequencies for naturally existing materials consequently [23-25]. Further, the tunability of the devices is other main parameter. For this purpose, liquid crystals (LCs) have been mostly used to manipulate the propagating THz wave properties due to the high birefringence and excellent electro-controllability in THz band [26, 27]. Correspondingly, in THz range, tunable absorbers, modulators, and switch devices have been reported by research groups [28-33].

To obtain of modulation depth and low insertion loss, between proposed devices in advanced THz communication systems, plasmonic devices is good candidate [32, 33]. Plasmonic device as a novel strategies for fast and tunable modulators were reported, recently [34-38].

The plasmonic gas sensor is one of main THz devices which are to be adapted to new technology and realm. In this paper, we present a new construction of gas sensors based on the plasmonic transmission (PT) effect used. To evaluate the proposed sensor and calculation of performance parameters including figure of merit and sensitivity, the effect of the different gas including Carbon Dioxide ($CO_2$), Acetonitrile ($C_2H_3N$), Carbon disulfide, and Sarin are considered. For this purpose 3D-FDTD method is considered. Our calculations show that by coupling between the incident waves and the surface plasmons of the structure, a high transmission ratio of 0.8 and relatively low insertion loss of 6 dB around the wavelength interval of 0.6-0.9 μm are achievable. Furthermore, the calculated sensitivity and figure of merit are 28 and 8.75, respectively.

The rest of the paper is organized as follows. In Section 2, the sensor structure is provided and geometrical and optical parameters are presented. In Section 3, the numerical method and the analytical formula of the proposed structure is studied. In Section 4, the results of numerical simulations and discussions are provided. Finally, the paper conclusion is provided in Section 5.

## 2. PROPOSED STRUCTURE

The 3D schematic of proposed structure is presented in Fig. 1. The structure is consisted of two-layer, $SiO_2$ and gold (Au) for the substrate and upper layer consequently. This design composed of three main sections: the light source inputs, top and substrate layer, hexagonal paths and two direct route inside the gold layer. Two direct route are include of two route; a main route, which is coupled with optical input source and a sub-route which is above the active region. In the gold layer is active path (shown with blue color) for coupling light and sensing gas parameter. Refractive index in each gas take into a section

side of hexagonal shape and with change of light peak output intensity, we achieved kind of gas. A branch of the hexagonal shape is shown in blue and is used to represent the refractive index of the gas, resulting in a change in light intensity for the PT effect. Also, in the following table, the geometrical parameters are provided. In the next section, we will describe the theoretical aspects of the present work.

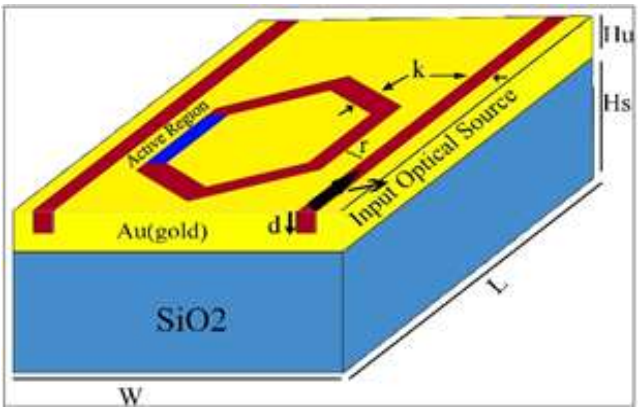


**Fig. 1.** 3D schematic of the designed structure for representation of gas sensor based on PT effect. The geometry dimensions are as follow: (L=1.14μm, W=0.712μm, Hs=0.95μm, Hu=0.155μm, k=0.05μm, d=0.105μm, r=0.025μm).

**TABLE 1.** GEOMETRICAL PARAMETERS OF THE PROPOSED STRUCTURE.

| Parameters | Value (μm) |
|---|---|
| L | 1.14 |
| W | 0.712 |
| Hs | 0.95 |
| Hu | 0.155 |
| k | 0.05 |
| d | 0.105 |
| r | 0.025 |

## 3. EQUATION EVALUATIONS

In this section, we illustrate the governing equation for the PT structure. In the previous section described the mechanism of PT, which is kwon of researcher. As can be seen the two layer structure is composed of a $SiO_2$ substrate and gold, which can operate as a PT sensor. When the light coupled in path horizontal, the corresponding incident can be coupled surface modes, and

propagated in hexagonal ring. Refractive index in the active region (blue market in the Fig.1) cause the light intensity output is change. This is the operation like mechanism the ring resonator.

The ring resonator structure includes two waveguides, which is placed on both sides of a ring resonator. (see Figure 1). Duty of one waveguide is to inject light to the resonator and the other one is responsible to couple light out of the resonator. As it is shown in Fig. 1, four ports can be introduced for this structure. The optical resonance can be observed at two output ports. First one at the other end of the input port is called through port (main-route). The transmission response of this port is similar to the through port of the all-pass filter, which means there is a dip at transmission of the through port at resonance wavelength. Second output that has reverse transmission response compared to through port is called drop port (sub-route). The transmission response of sub and main port resonators is expressed by following equations [39].

$$T_{Through} = \frac{r_2^2 a^2 - 2r_1 r_2 a\cos\varphi + r_1^2}{1 - 2r_1 r_2 a\cos\varphi + (r_1 r_2 a)^2} \qquad (1)$$

$$T_{Drop} = \frac{(1 - r_1^2)(1 - r_1^2)a}{1 - 2r_1 r_2 a\cos\varphi + (r_1 r_2 a)^2}$$

Where $r_1$ and $r_2$ are self-coupling coefficients of the first and second couplers, respectively. And φ is phase shift of the light after one round-trip inside the ring, is amount of diminution of light after one round trip. In the other hand, resonance mod in the ring depend on the coupling coefficients which is change of refractive index. These changes is in the active region in branch of hexagonal.

Now, in what follow the optical properties of the each layer are presented. The substrate dielectric is silicon oxide ($SiO_2$) with dielectric constant of $\epsilon$=2.43. The use of $SiO_2$ increases the propagation length of surface plasmon by significantly reduce the propagation loss [40]. In the upper layer is gold which created two horizontal path for couple light source. Gold is selected as the metal film due to its low intrinsic loss in the optical spectral regime. The gold has a complex permittivity, ε, with frequency dependence described by the Drude model [41-46].

$$\epsilon_m = \epsilon' + i\epsilon'' = 1 - \frac{\omega_p^2}{(\omega^2+\gamma^2)} + \frac{i\gamma\omega_p^2}{\omega(\omega^2+\gamma^2)} \quad (2)$$

Here $\omega_p$ and ɣ, in the Drude model, is the plasmon frequency and damping rate, respectively.

So we can calculate the output profile by having the layers characteristics by applying the light source. In the other words, this mechanism shows the transmission and reflection difference of light is proportional to the gas refractive index in the hexagonal side. In addition, the next section reveals that with changes in the refractive index of the hexagonal side, peak intensity changes.

In the following, performance parameters of the proposed structure including figure of merit (FoM) and sensitivity is provided. FoM refers to performance parameter of the device and calculated through FoM= {(Δn/ΔT)/T} in which (Δn/ΔT) refers to transmission shift, and T is transmission at specific wavelength. Also, sensitivity as a main parameter of sensor is S= (Δλ/Δn), where Δλ and Δn are wavelength shift and refractive index change, respectively.

## 4. SIMULATION RESULTS AND DISCUSSIONS

In this section, the results of the simulations for the gas within the active region are presented. Simulations have been performed based on the Equations (1). The system of equations solved using numerical method of finite difference time domain (FDTD). As mentioned in earlier section, PT gas sensor behavior in the structure is proportional with peak light intensity for different gases. So, in order to change the output light intensity in our proposed sensor, the infiltration gas through the active region should be changed. To do this, we examine different gases infiltration in the active region. The optical properties of different gases used in our simulations are listed in Table 2. This table give the refractive index of different gases. Previously discussed the importance of gas detection. This table lists all gases that can be used in several types. Carbon Dioxide ($CO_2$), Acetonitrile ($C_2H_3N$), Carbon disulfide ($CS_2$), and Sarin gas are very dangerous and detection of them is very important.

**TABLE 2** PHYSICAL PROPERTIES OF COMMON GASES

| Gas | Refractive index | Reference |
|---|---|---|
| $CO_2$(Carbon Dioxide) | ng=1.000467 | Bideau-Mehu et al. 1973 |
| C2H3N (Acetonitrile) | ng = 1.3560 | Moutzouris et al.2014 |
| CS2 (Carbon disulfide) | ng = 1.7259 | Kedenburg et al. 2012 |
| Sarin | ng = 1.366 | Rheims et al. 1997 |

As an example, the peak light transmission for $CO_2$ gas in the main route are shown at different wavelength in Fig. 2a. In this case, with injection the $CO_2$ gas in active region light transmission in two peaks. Two peaks shown in the figure are used for each type of gas. Of course, these peaks, for each gas, have their own wavelengths. This is also very useful in detecting accuracy and selectivity sensitivity.

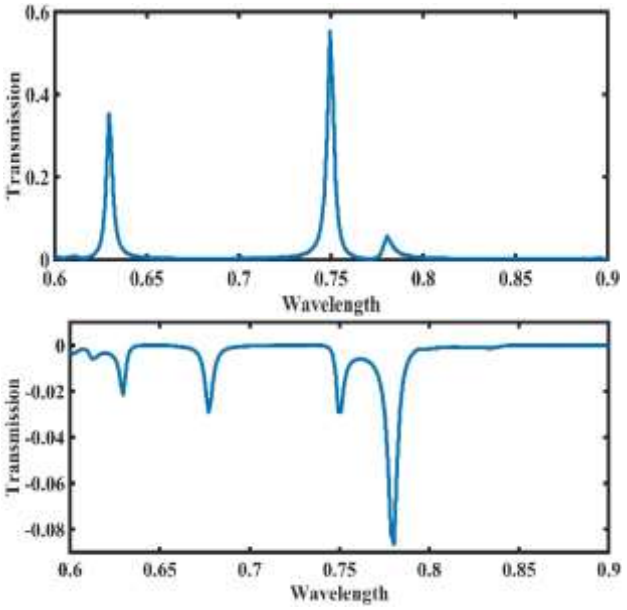


**Fig. 2.** The variation of light transmission versus wavelength (nm) with the injection CO2 gas in active layer. (a). shown on the main routee and (b). on the sub-routee.

Light transmission is obtained for two route, main and sub-route, for increase detection sensitivity. This is special for every gas. For example, for $CO_2$ gas,

this amount is plotted in sub-route. The sensitivity and resolution increases with presence of two curves for the light transmission, which to determine the type of gas. Therefore, with two outputs in the sensor, the diagnosis is better for each gas type.

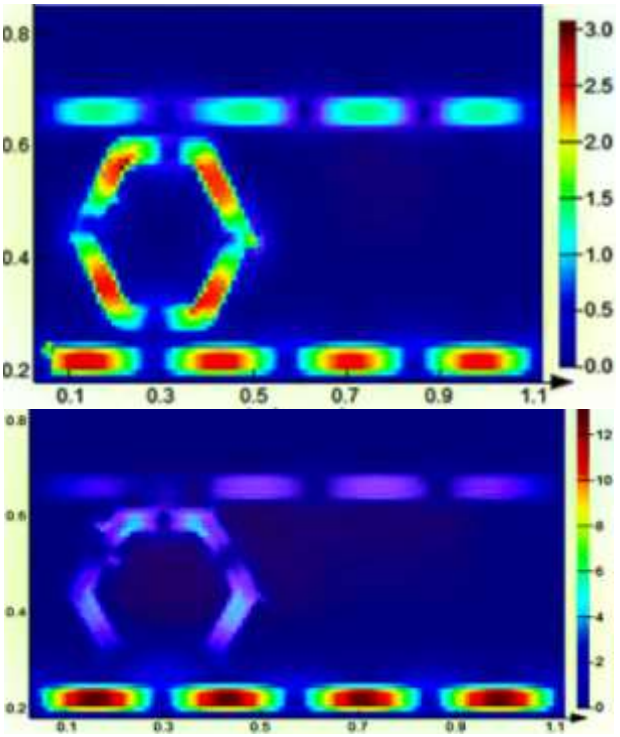


**Fig. 3.**(a) The distribution field profile of the sensor with the infiltration of $CO_2$ in the active region. (b) field profile of the sensor with the infiltration of $CS_2$ with high refractive index in the active region.

In the next step, distribution field profile of the sensor is plotted for two different gases at 760 nm wavelength. This profile is shown for $CO_2$ gas in Figure 3.a. The distribution of the field in two routes is quite clear. In this state, the coupling of light in a hexagonal reing is well represented. This condition for $CS_2$ is shown in Figure. 3b. As can be seen, light transmission is special for different gases in the every wavelength. The distribution of the field in the path and the surface of the hexagonal paths is similar to the ring resonator. Which, for any specific refractive index in the active region, causes the field to be coupled in the hexagonal paths, as well as changes in the main and sub-route.

This mechanism clearly be seen in Figure 3.
In the next case, the simulation result for different gases in the Table.1, is provided. As shown in this figure, the intensity of the transmitted light output is different for each gas. Of course, these changes have two peaks at the outlet for some gases. The presence of two peaks in the output changes shows the high sensitivity and selectivity of the sensor. Which can be said that each gas has its own output profiles. The variation in the intensity of the output transmitted light and the number of peaks represent the refractive index of each gas. Therefore, detection of the desired gas is achievable. High efficiency and sensitivity, high speed, accuracy and selectivity to detect type are gases, the advantages of this sensor. In addition, the other advantage of this sensor is the low input intensity that eliminates sensitivity to nonlinear factors.

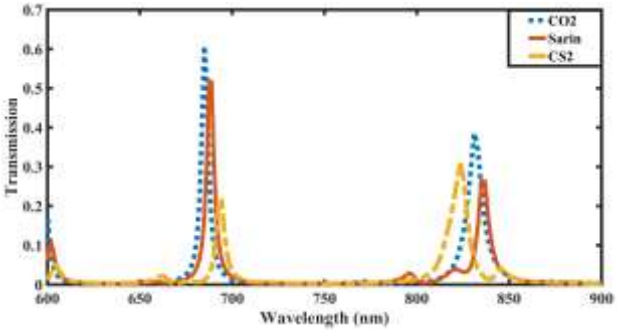


**Fig. 4.** The variation of light transmission versus wavelength with the injection different gases in active layer. With change of the refractive index gases, the peak intensity transmission is change consequently.

In this way the light intensity transmitted is plotted for different gases. The refractive index range for most gases is between 1 and 2. Therefore, the intensity of the output of a refractive index plotted for this range. As mentioned in the previous section for each gas intensity is the two output peaks. In the main route has two peaks. Of course, this is done at each specific wavelength. Because of this, we plot the intensity for each peak in the wavelength range. Figure 5.a is plotted for the first peak of all gases in the wavelength range of 685 to 700 nm. Clearly be seen that for any gas is particular. The intensity of the output light in the main path has two peaks. For the second peak, it is also plotted in all gases for the wavelength range of 825 to 830 nm. So, as shown in the Fig. 5.b, the output intensity for each gas is particular. For example, for the Sarin gas, the intensity of the light output of the first peak is 0.55, and 0.27 for the second peak. This carefully choose the type of gas.

The performance parameters including sensitivity and FoM are introduced in the following. As can be seen from Fig. 4. maximum of sensitivity is near of 28, and maximum FoM is 8.75.

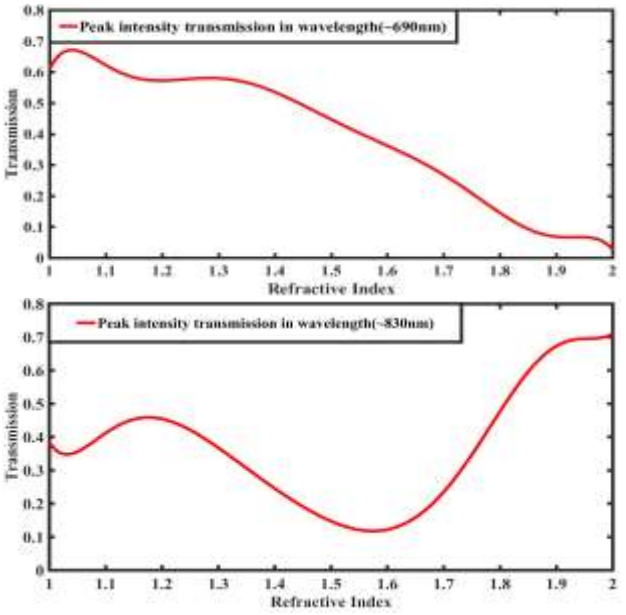


**Fig. 5.** The variation of light transmission versus refractive index for different gases in active layer. (a). First peak light intensity for main route and (b). For sub-route with change of the refractive index gases, the two peaks intensity transmission is change consequently.

**TABLE 3**

A COMPARISON TABLE OF SEVERAL DIFFERENT WORK GAS SENSOR BASED ON PLASMONIC.

| Ref | Structure | Tunable | Integrable |
|---|---|---|---|
| [47] | Fiber Optic | No | No |
| [48] | IMI | No | No |
| [49] | Fiber Optic | No | No |
| This work | IMI | Yes | Yes |

In Table 3, we examine and compare several gas sensors. Requiring miniaturization, high performance, high sensitivity, flexibility range and of non-noise, parameters of a sensor is working properly. The correct detection for sensors is one of the most important parameters.

Toxic gas detection is essential to deal with it. Used for treatment and prevention of pollution in the environment is also important. The proposed sensor, despite its limited availability, is suitable for use in today's technology. Finally, considering the performance parameters of gas sensors, new structures such as carbon nanotubes and with high sensitivity properties is needed [50-57].

## 5. CONCLUSION

A nano-scale plasmonic gas sensor based on the plasmonic transmission effect at visible frequencies was presented here. By considering the optical properties of plasmonic materials, four types of gases including $CO_2$, $C_2H_3N$, $CS_2$, and Sarin were studied. To enhance the performance parameters, the coupling between the incident light and the surface plasmons as well as their polarization dependence have been considered. Our calculations shown that by coupling between the incident waves and the surface plasmons of the structure, a high transmission ratio of 0.8 and relatively low insertion loss of 6 dB around the wavelength interval of 0.6-0.9 μm were achievable. In addition, the calculated sensitivity and figure of merit are 28 and 8.75, respectively. Our presented nano-scale gas sensor is suitable for practical on-chip applications.

## REFERENCES

[1] Dolatabady, Alireza, Somayyeh Asgari, and Nosrat Granpayeh. *Tunable mid-infrared nanoscale graphene-based refractive index sensor*. IEEE Sensors Journal 18.2 (2017): 569-574. Available: https://doi.org/ 10.1109/JSEN.2017.2778003

[2] Davoodi, Fatemeh, and Nosrat Granpayeh. *Nonlinear Graphene-Transition Metal Dichalcogenides Heterostructure Refractive Index Sensor*. IEEE Sensors Journal (2019). Available: https://doi.org/10.1109/JSEN.2019.2897345

[3] Amiri, Samira, and Najmeh Nozhat. *Plasmonic nanodipole antenna array with extra arms for sensing applications.* JOSA B 33.8 (2016): 1769-1776. Available: https://doi.org/10.1364/JOSAB.33.001769

[4] Salemizadeh, Mehrnoosh, Fatemeh Fouladi Mahani, and Arash Mokhtari. *Design of aluminum-based nanoring arrays for realizing efficient plasmonic sensors*. JOSA B 36.3 (2019): 786-793. Available: https://doi.org/10.1364/JOSAB.36.000786

[5] Neshat, Mohammad, et al. *Whispering-gallery-mode resonance sensor for dielectric sensing of drug tablets*. Measurement Science and Technology 21.1 (2009): 015202. Available: https://doi.org/10.1088/0957-0233/21/1/015202

[6] Madadi, Zahra, et al. *An Infrared Narrow-band Plasmonic Perfect Absorber as a Sensor*. Optik (2019). Available: https://doi.org/10.1016/j.ijleo.2019.02.078

[7] Abbasi, Mohammad, Mohammad Soroosh, and Ehsan Namjoo. *Polarization-insensitive temperature sensor based on liquid filled photonic crystal fiber*. Optik 168 (2018): 342-347. Available: https://doi.org/10.1016/j.ijleo.2018.04.116

[8] Khadem, SM Jebreiil, et al. *Investigating the effect of gas absorption on the electromechanical and electrochemical behavior of graphene/ZnO structure, suitable for highly selective and sensitive gas sensors*. Current Applied Physics 14.11 (2014): 1498-1503. Available: https://doi.org/10.1016/j.cap.2014.07.020

[9] Olyaee, Saeed, Hassan Arman, and Alieh Naraghi. *Design, simulation, and optimization of acetylene gas sensor using hollow-core photonic bandgap fiber*. Sensor Letters 13.5 (2015): 387-392.

[10] Ebnali-Heidari, Majid, et al. *Designing tunable microstructure spectroscopic gas sensor using optofluidic hollow-core photonic crystal fiber*. IEEE Journal of Quantum Electronics50.12 (2014): 1-8. Available: https://doi.org/10.1109/JQE.2014.2362353

[11] Fard, Shokooh Khalili, Sara Darbari, and Vahid Ahmadi. *Electro-Plasmonic Gas Sensing Based on Reduced Graphene Oxide/Ag Nanoparticle Heterostructure*. IEEE Sensors Journal 18.14 (2018): 5770-5777. Available: https://doi.org/10.1109/JSEN.2018.2842081

[12] Salimpour, Saman, and Hassan Rasooli Saghai. *Impressive Reduction of Dark Current in InSb Infrared Photodetector to achieve High Temperature Performance*. Journal of Optoelectronical Nanostructures 3.4 (2018): 81-96. Available: http://jopn.miau.ac.ir/article_3265.html

[13] Faezinia, Hamid. *Quantum modeling of light absorption in graphene based photo-transistors*. Journal of Optoelectronical Nanostructures 2.1 (2017): 9-20. Available: http://jopn.miau.ac.ir/article_2196.html

[14] Minabi, Hosseini, et al. *The effect of temperature on optical absorption cross section of bimetallic core-shell nano particles*. Journal of Optoelectronical Nanostructures 1.3 (2016): 67-76. Available: http://jopn.miau.ac.ir/article_2203.html

[15] Farmani, Ali, et al. *Design of a tunable graphene plasmonic-on-white graphene switch at infrared range*. Superlattices and Microstructures 112 (2017): 404-414. Available: https://doi.org/10.1016/j.spmi.2017.09.051

[16] Farmani, Ali, Mehdi Miri, and Mohammad Hossein Sheikhi. *Design of a high extinction ratio tunable graphene on white graphene polarizer*. IEEE Photonics Technology Letters 30.2 (2018): 153-156. Available: https://doi.org/10.1109/LPT.2017.2779160

[17] Farmani, Ali, Mehdi Miri, and Mohammad H. Sheikhi. *Tunable resonant Goos–Hänchen and Imbert–Fedorov shifts in total reflection of terahertz beams from graphene plasmonic metasurfaces*. JOSA B 34.6 (2017): 1097-1106. Available: https://doi.org/10.1364/JOSAB.34.001097

[18] Moftakharzadeh, Ali, Behnaz Afkhami Aghda, and Mehdi Hosseini. *Noise Equivalent Power Optimization of Graphene-Superconductor Optical Sensors in the Current Bias Mode*. Journal of Optoelectronical Nanostructures 3.3 (2018): 1-12. Available: http://jopn.miau.ac.ir/article_3040.html

[19] Rezvani, Masoud, and Maryam Fathi Sepahvand. *Simulation of Surface Plasmon Excitation in a Plasmonic Nano-Wire Using Surface Integral Equations*. Journal of Optoelectronical Nanostructures 1.1 (2016): 51-64. Available: http://jopn.miau.ac.ir/article_1815.html

[20] Servatkhah, Mojtaba, and Hadi Alaei. *The Effect of Antenna Movement and Material Properties on Electromagnetically Induced Transparency in a Two-Dimensional Metamaterials*. Journal of Optoelectronical Nanostructures 1.2 (2016): 31-38. Available: http://jopn.miau.ac.ir/article_2046.html

[21] Dhillon, S. S., et al. *The 2017 terahertz science and technology roadmap*. Journal of Physics D: Applied Physics 50.4 (2017): 043001. Available: doi:10.1088/1361-6463/50/4/043001

[22] Hangyo, Masanori. *Development and future prospects of terahertz technology*. Japanese Journal of Applied Physics 54.12 (2015): 120101. Available: https://doi.org/10.7567/JJAP.54.120101

[23] Lee, In-Sung, et al. *Optical isotropy at terahertz frequencies using anisotropic metamaterials*. Applied Physics Letters 109.3 (2016): 031103. Available: https://doi.org/10.1063/1.4959032

[24] Sanphuang, Varittha, et al. *THz transparent metamaterials for enhanced spectroscopic and imaging measurements*. IEEE Trans. THz Sci. Technol 5.1 (2015): 117-123. Available: https://doi.org/10.1109/TTHZ.2014.2362659

[25] Pan, Ci-Ling, et al. *Control of enhanced THz transmission through metallic hole arrays using nematic liquid crystal*. Optics express 13.11 (2005): 3921-3930. Available: https://doi.org/10.1364/OPEX.13.003921

[26] Wang, Lei, et al. *Broadband tunable liquid crystal terahertz waveplates driven with porous graphene electrodes*. Light: Science & Applications 4.2 (2015): e253. Available: https://doi.org/10.1038/lsa.2015.26

[27] Du, Yan, et al. *Electrically tunable liquid crystal terahertz phase shifter driven by transparent polymer electrodes*. Journal of Materials Chemistry C 4.19 (2016): 4138-4142. Available: https://doi.org/10.1039/C6TC00842A

[28] Isić, Goran, et al. *Electrically tunable critically coupled terahertz metamaterial absorber based on nematic liquid crystals*. Physical Review Applied 3.6 (2015): 064007. Available: https://doi.org/10.1103/PhysRevApplied.3.064007

[29] Kowerdziej, Rafał, et al. *Terahertz characterization of tunable metamaterial based on electrically controlled nematic liquid crystal*. Applied Physics Letters 105.2 (2014): 022908. Available: https://doi.org/10.1063/1.4890850

[30] Decker, Manuel, et al. *Electro-optical switching by liquid-crystal controlled metasurfaces*. Optics express 21.7 (2013): 8879-8885. Available: https://doi.org/10.1364/OE.21.008879

[31] Shrekenhamer, David, Wen-Chen Chen, and Willie J. Padilla. *Liquid crystal tunable metamaterial absorber*. Physical review letters 110.17 (2013): 177403. Available: https://doi.org/10.1103/PhysRevLett.110.177403

[32] Chen, Chia-Chun, et al. *Continuously tunable and fast-response terahertz metamaterials using in-plane-switching dual-frequency liquid crystal cells*. Optics letters 40.9 (2015): 2021-2024. Available: https://doi.org/10.1364/OL.40.002021

[33] Savo, Salvatore, David Shrekenhamer, and Willie J. Padilla. *Liquid crystal metamaterial absorber spatial light modulator for THz applications*. Advanced Optical Materials 2.3 (2014): 275-279. Available: https://doi.org/10.1002/adom.201300384

[34] Etcheverry, Sebastián, et al. *Microsecond switching of plasmonic nanorods in an all-fiber optofluidic component.* Optica 4.8 (2017): 864-870. Available: https://doi.org/10.1364/OPTICA.4.000864

[35] Etcheverry, Sebastián, et al. *Digital electric field induced switching of plasmonic nanorods using an electro-optic fluid fiber*. Applied Physics Letters 111.22 (2017): 221108. Available: https://doi.org/10.1063/1.5001702

[36] Zhang, Kun, et al. *Dual-mode electromagnetically induced transparency and slow light in a terahertz metamaterial*. Optics letters 39.12 (2014): 3539-3542. Available: https://doi.org/10.1364/OL.39.003539

[37] Zhang, Fuli, et al. *Polarization and incidence insensitive dielectric electromagnetically induced transparency metamaterial*. Optics express 21.17 (2013): 19675-19680. Available: https://doi.org/10.1364/OE.21.019675

[38] Wang, Jing, et al. *Liquid crystal terahertz modulator with plasmon-induced transparency metamaterial.* Optics express 26.5 (2018): 5769-5776. Available: https://doi.org/10.1364/OE.26.005769

[39] Bogaerts, Wim, et al. *Silicon microring resonators*. Laser & Photonics Reviews 6.1 (2012): 47-73. Available: https://doi.org/10.1088/2040-8986/aaba20

[40] Farmani, Ali, Mehdi Miri, and Mohammad H. Sheikhi. *Analytical modeling of highly tunable giant lateral shift in total reflection of light beams from a graphene containing structure.* Optics Communications 391 (2017): 68-76. Available: https://doi.org/10.1016/j.optcom.2017.01.018

[41] Farmani, Ali. *Three-dimensional FDTD analysis of a nanostructured plasmonic sensor in the near-infrared range*. JOSA B 36.2 (2019): 401-407. Available: https://doi.org/10.1364/JOSAB.36.000401

[42] Baqir, M. A., et al. *Nanoscale, tunable, and highly sensitive biosensor utilizing hyperbolic metamaterials in the near-infrared range*. Applied optics 57.31 (2018): 9447-9454. Available: https://doi.org/10.1364/AO.57.009447

[43] Farmani, Ali, Ali Mir, and Zhaleh Sharifpour. *Broadly tunable and bidirectional terahertz graphene plasmonic switch based on enhanced Goos-Hänchen effect.*

Applied Surface Science 453 (2018): 358-364. Available: https://doi.org/10.1016/j.apsusc.2018.05.092

[44] Farmani, Ali, et al. *Highly sensitive nano-scale plasmonic biosensor utilizing Fano resonance metasurface in THz range: numerical study*. Physica E: Low-dimensional Systems and Nanostructures 104 (2018): 233-240. Available: https://doi.org/10.1016/j.physe.2018.07.039

[45] Farmani, Ali. *Quantum-dot semiconductor optical amplifier: performance and application for optical logic gates*. Majlesi Journal of Telecommunication Devices 6.3 (2017). Available: http://journals.iaumajlesi.ac.ir/td/index/index.php/td/article/view/428

[46] Nejad, Hamed Emami, Ali Mir, and Ali Farmani. *Supersensitive and Tunable Nano-Biosensor for Cancer Detection.* IEEE Sensors Journal (2019). Available: https://doi.org/10.1109/JSEN.2019.2899886

[47] Mishra, Satyendra K., Deepa Kumari, and Banshi D. Gupta. *Surface plasmon resonance based fiber optic ammonia gas sensor using ITO and polyaniline*. Sensors and Actuators B: Chemical 171 (2012): 976-983. Available: https://doi.org/10.1016/j.snb.2012.06.013

[48] Rodrigo, Sergio G. *Terahertz gas sensor based on absorption-induced transparency*. EPJ Applied Metamaterials 3 (2016): 11. Available: https://doi.org/10.1051/epjam/2016013

[49] Sultan, Murtadha Faaiz, Ali A. Al-Zuky, and Shehab A. Kadhim. *Surface Plasmon Resonance Based Fiber Optic Sensor: Theoretical Simulation and Experimental Realization.* Al-Nahrain Journal of Science 21.1 (2018): 65-70. Available: http://anjs.edu.iq/index.php/anjs/article/view/156

[50] Farmani, Ali, and Ali Mir. *Graphene Sensor based on Surface Plasmon Resonance for Optical Scanning*. IEEE Photonics Technology Letters (2019). Available: https://doi.org/ 10.1109/LPT.2019.2904618

[51] Ghodrati, Maryam, Ali Farmani, and Ali Mir. *Nanoscale Sensor-based Tunneling Carbon Nanotube Transistor for Toxic Gases Detection: A First-Principle Study*. IEEE Sensors Journal (2019). Available: https://doi.org/10.1109/JSEN.2019.2916850

[52] Heidari, Ebrahim. *Ultra-Relativistic Solitons with Opposing Behaviors in Photon Gas Plasma*. Journal of Optoelectronical Nanostructures 4.1 (2019): 27-38. Available: http://jopn.miau.ac.ir/article_3383.html

[53] Pourchitsaz, Kazem, and Mohammad Reza Shayesteh. *Self-heating effect modeling of a carbon nanotube-based fieldeffect transistor (CNTFET).* Journal of Optoelectronical Nanostructures 4.1 (2019): 51-66. Available: http://jopn.miau.ac.ir/article_3383.html

[54] Karachi, Nima, Masoomeh Emadi, and Mojtaba Servatkhah. *Computational Investigation on Structural Properties of Carbon Nanotube Binding to Nucleotides*

*According to the QM Methods*. Journal of Optoelectronical Nanostructures 4.1 (2019): 99-124. Available: http://jopn.miau.ac.ir/article_3388.html

[55] Nayeri, Mahdieh, and Maryam Nayeri. *A Novel Design of Penternary Inverter Gate Based on Carbon Nano Tube*. Journal of Optoelectronical Nanostructures 3.1 (2018): 15-26. Available: http://jopn.miau.ac.ir/article_2820.html

[56] Keleshtery, M. Hassani, Hassan Kaatuzian, and Ali Mir. *Analysis and investigation of slow light based on plasmonic induced transparency in metal-dielectric-metal ring resonator in a waveguide system with different geometrical designs*. Opt. Photon. J. 6.8 (2016): 177-184. Available: https://www.scirp.org/journal/PaperInforCitation.aspx?PaperID=70325

[57] Jafari, Azin, and Amir Amini. *Lactic acid gas sensor based on polypyrrole thin film.* Materials Letters 236 (2019): 175-178. Available: https://doi.org/10.1016/j.matlet.2018.10.066